SOLPS modeling of impurity seeded plasmas in ASDEX Upgrade

F. Hitzler[1,2], M. Wischmeier[1], F. Reimold[3], M. Bernert[1], A. Kallenbach[1], D. P. Coster[1], the ASDEX Upgrade Team[4] and the EUROfusion MST1 Team[5]

[1] *Max-Planck-Institut für Plasmaphysik, 85748 Garching, Germany*

[2] *Physik-Department E28, Technische Universität München, 85747 Garching, Germany*

[3] *Forschungszentrum Jülich, 52425 Jülich, Germany*

[4] *See author list "A. Kallenbach et al., 2017 Nucl. Fusion 57 102015"*

[5] *See author list "H. Meyer et al., 2017 Nucl. Fusion 57 102014"*

Introduction

Power exhaust will be a critical issue in future fusion devices. The technological limits for the stationary divertor power loads are below $\sim 10\,\mathrm{MWm}^{-2}$ [1]. To reduce the erosion of target materials the target temperatures need to stay below $\sim 5\,\mathrm{eV}$ [2]. In an unmitigated scenario these limits will easily be exceeded. This can be prevented by controlled seeding of impurity species like argon or nitrogen. Such impurities lead to radiative power dissipation via line radiation which results in strongly reduced divertor target temperatures and power loads. For the operation of future fusion devices it is crucial to identify an operational window in which the limits stated above are satisfied but at the same time the impact on the confined plasma is as low as possible. For this purpose different impurity seeding scenarios are investigated in this work via SOLPS 5.0 modeling in order to ensure no detrimental impact on the burn conditions.

SOLPS 5.0 modeling

The SOLPS 5.0 (*Scrape-off layer plasma simulation*) code package is a combination of the fluid plasma code B2.5 and the Monte-Carlo neutral transport code EIRENE [3]. The computational mesh of the simulations shown in this work is based on the magnetic equilibrium of the ASDEX Upgrade H-mode shot 29256 [4]. Experimentally motivated the input power (i.e. the power crossing the core boundary) is set to 5 MW and the deuterium fueling rate is feedback controlled to sustain an electron density at the outer midplane separatrix of $2.5 \cdot 10^{19}\,\mathrm{m}^{-3}$. In order to reproduce the experimental H-mode upstream profiles of density and temperature the perpendicular diffusive transport coefficients were adjusted in [4] and are kept constant during this work. Drifts and neo-classical transport effects are neglected. As a convergence criterion for the steady state simulations it is required that important plasma parameters like density, temperature, energy and particle fluxes are settled at constant values. Another important convergence criterion is the particle balance (i.e. the discrepancy between particle fueling and pumping). The

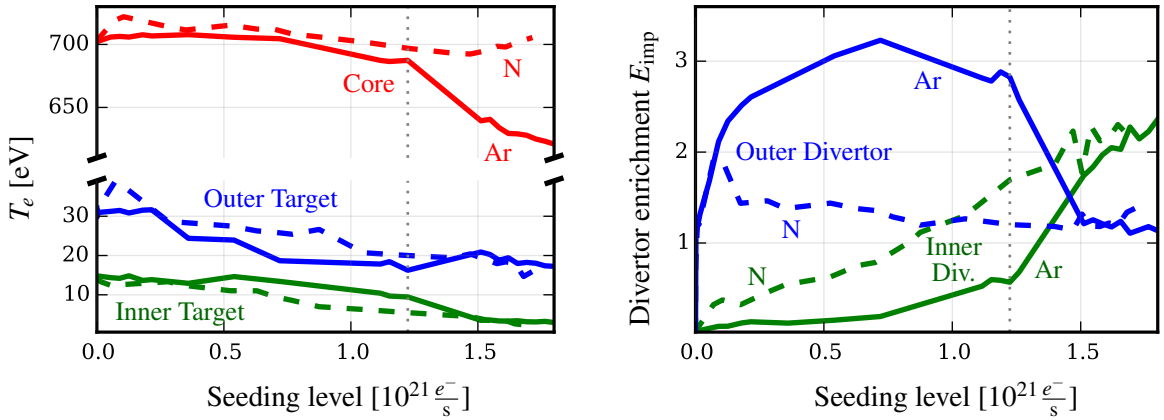

Figure 1: *Evolution of the electron temperature (left) and the divertor enrichment (right) with increasing impurity seeding levels in different regions. Solid lines show the Ar seeding scan, dashed lines show the N seeding scan. The vertical dotted lines mark the position at which the change in the Ar density distribution described below is observed* ($\sim 1.22 \cdot 10^{21} \frac{e^-}{s}$).

simulations in this work are only considered as converged if the deuterium particle balance is below 5 %. However, in a few cases especially for impurity species and at low particle throughput it is observed that the particle balance is deficient and exceeds this limit considerably.

Numerical impurity seeding scans

In order to investigate different impurity seeding scenarios seeding scans using argon (Ar) and nitrogen (N) have been performed. With the presented modeling setup total impurity radiation fractions of up to $\sim 60\,\%$ of the input power (5 MW) could be achieved at the maximum achievable impurity seeding levels. At seeding levels above $\sim 1.8 \cdot 10^{21} \frac{e^-}{s}$ (in electron equivalent units) the simulations fail as the input power of 5 MW is not sufficient anymore to sustain the high impurity radiation fractions.

Figure 1 (left) shows the peak T_e at the inner and outer divertor targets (green / blue) and the average T_e in the confined region (red), i.e. in the innermost flux surface in the computational domain at $\rho_{pol} \approx 0.9$. The impurity seeding scans are shown in solid lines for Ar and in dashed lines for N. As expected the radiative power dissipation leads to decreasing temperatures in all regions. However, the impact of the Ar impurities on the confined region is much stronger than for N. At high seeding rates we observe a T_e drop of up to $\sim 12\,\%$ for Ar and $\sim 2\,\%$ for N compared to the unseeded reference. This is due to the higher radiation efficiency of Ar, especially in hotter regions like in the core, see Fig. 2. Only at temperatures below ~ 5 eV N is a more efficient radiator. On the other hand according to Fig. 1 Ar leads to a stronger reduction of the target T_e in the outer divertor, while N is more beneficial in the inner divertor. This can be explained by differences in the impurity density distributions or by the divertor enrichment which is defined as the ratio of the average impurity concentration in the divertor to the impurity concentration in the

core: $E_{\mathrm{imp}} = \frac{c_{\mathrm{imp,div}}}{c_{\mathrm{imp,core}}}$. A high enrichment indicates a good confinement of the impurity in the divertor region and is required to minimize the impact on the confined plasma whilst keeping high radiative losses in the divertor. As it can be seen on the right side in Fig. 1 in most of the seeding range Ar exhibits a stronger divertor enrichment in the outer divertor (blue), and N has a better enrichment in the inner divertor (green). However, above an Ar seeding rate of $1.22 \cdot 10^{21} \frac{e^-}{\mathrm{s}}$ (dotted vertical lines) we observe a different Ar density distribution which is shifted from the outer to the inner divertor. This also results in the drop of the Ar divertor enrichment in the outer divertor and in a strong increase in the inner divertor. For the N impurities no considerable change in the density distribution is observed and the densities increase steadily in all regions with particularly high densities in the inner divertor from early on.

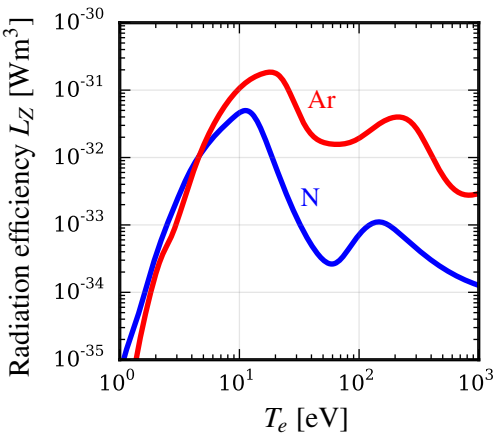

Figure 2: *Radiation efficiencies of Ar and N in coronal equilibrium at* $n_e = 10^{19}\,\mathrm{m}^{-3}$ *according to the ADAS database [5].*

Force Analysis

To investigate the change in the Ar density distribution described above, the parallel forces acting on the impurities along the flux tubes are analyzed. While the pressure gradient force and the electrostatic force only have a small impact on the impurities in the presented simulations, the main drivers for the impurity redistribution are the friction and thermal forces [6]. These forces are shown in Fig. 3 along different flux tubes in the scrape-off layer (SOL) for two different Ar seeding cases where strong friction and thermal forces arise in the high seeding case. On the high field side the forces practically compensate each other, while around the outer midplane a significant net force develops (see black lines). In the flux tube close to the separatrix the net force (directed towards the inner divertor) is reduced by $\sim 22\,\%$ at high seeding. However, in the far SOL the direction of the net force is reversed going from low to high seeding conditions, pointing towards the outer and inner target respectively. Therefore, the different Ar density distribution seems to be due to the change of the friction and thermal forces in the far SOL.

Conclusion

For the operation of future fusion devices it will be crucial to identify an impurity seeding scenario which allows an optimization of the plasma performance in terms of both power exhaust and confinement. To achieve this, one can investigate the potential of mixing different impurity species to exploit the differences in the radiation efficiency, impurity density distribu-

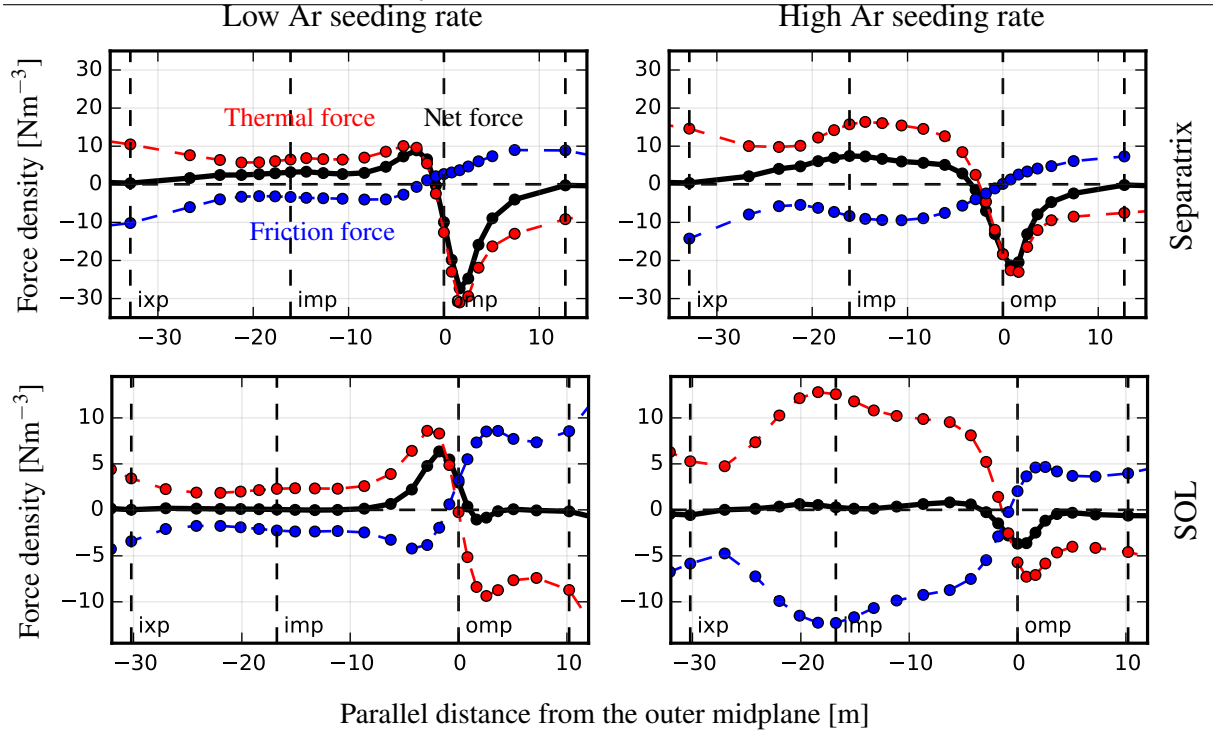

Figure 3: *Parallel friction and thermal forces acting on the Ar impurities in the scrape-off layer (SOL) plotted along two different fluxtubes. Negative values indicate forces towards the inner divertor, positive values towards the outer divertor. The plots on the left show a case with low Ar seeding level* ($\sim 1.15 \cdot 10^{21} \frac{e^-}{\mathrm{s}}$)*, and the plots on the right show a case with high Ar seeding level* ($\sim 1.51 \cdot 10^{21} \frac{e^-}{\mathrm{s}}$)*. On top the fluxtube closest to the separatrix is shown* ($\Delta s_{\mathrm{omp}} = 0.42\,\mathrm{mm}$) *while on the bottom a fluxtube further in the SOL is shown* ($\Delta s_{\mathrm{omp}} = 5.7\,\mathrm{mm}$)*. The dashed vertical marker lines denote the inner x-point, inner midplane, outer midplane and outer x-point positions.*

tion and divertor enrichment. In the simulations presented in this work (neglecting drift terms) the observed change of the Ar density distribution at high seeding rates is caused by a change in the parallel friction and thermal forces. Additionally, a shift of the impurity ionization front away from the target is observed in the simulations which might also contribute to the changing density distribution via a reduced impurity retention in the divertor. However, it will be crucial to investigate how the impurity density distributions are affected when drift terms are included which are known to influence the particle balance in the divertor [7].

This work has been carried out within the framework of the EUROfusion Consortium and has received funding from the Euratom research and training program 2014-2018 under grant agreement number 633053. The views and opinions expressed herein do not necessarily reflect those of the European Commission.

References

[1] A. Loarte, Nucl. Fusion **47** (2007)

[2] A. Kallenbach, PPCF **55** (2013)

[3] R. Schneider, Contrib. Plasma Phys. **46** (2006)

[4] L. Xiang, Nucl. Mater. Energy **12** (2017)

[5] H. P. Summers, The ADAS user manual (2004)

[6] P. C. Stangeby, The Plasma Boundary of Magnetic Fusion Devices (2000)

[7] F. Reimold, Nucl. Mater. Energy **12** (2017)